

Centrality Dependence of the High p_T Charged Hadron Suppression in Au+Au Collisions at

$$\sqrt{s_{NN}} = 130 \text{ GeV}$$

K. Adcox,⁴⁰ S. S. Adler,³ N. N. Ajitanand,²⁷ Y. Akiba,¹⁴
 J. Alexander,²⁷ L. Aphecetche,³⁴ Y. Arai,¹⁴ S. H. Aronson,³
 R. Averbeck,²⁸ T. C. Awes,²⁹ K. N. Barish,⁵ P. D. Barnes,¹⁹
 J. Barrette,²¹ B. Bassalleck,²⁵ S. Bathe,²² V. Baublis,³⁰
 A. Bazilevsky,^{12,32} S. Belikov,^{12,13} F. G. Bellaiche,²⁹ S. T. Belyaev,¹⁶
 M. J. Bennett,¹⁹ Y. Berdnikov,³⁵ S. Botelho,³³ M. L. Brooks,¹⁹
 D. S. Brown,²⁶ N. Bruner,²⁵ D. Bucher,²² H. Buesching,²²
 V. Bumazhnov,¹² G. Bunce,^{3,32} J. Burward-Hoy,²⁸ S. Butsyk,^{28,30}
 T. A. Carey,¹⁹ P. Chand,² J. Chang,⁵ W. C. Chang,¹ L. L. Chavez,²⁵
 S. Chernichenko,¹² C. Y. Chi,⁸ J. Chiba,¹⁴ M. Chiu,⁸
 R. K. Choudhury,² T. Christ,²⁸ T. Chujo,^{3,39} M. S. Chung,^{15,19}
 P. Chung,²⁷ V. Cianciolo,²⁹ B. A. Cole,⁸ D. G. D'Enterria,³⁴
 G. David,³ H. Delagrange,³⁴ A. Denisov,¹² A. Deshpande,³²
 E. J. Desmond,³ O. Dietzsch,³³ B. V. Dinesh,² A. Drees,²⁸
 A. Durum,¹² D. Dutta,² K. Ebisu,²⁴ Y. V. Efremenko,²⁹
 K. El Chenawi,⁴⁰ H. En'yo,^{17,31} S. Esumi,³⁹ L. Ewell,³ T. Ferdousi,⁵
 D. E. Fields,²⁵ S. L. Fokin,¹⁶ Z. Fraenkel,⁴² A. Franz,³
 A. D. Frawley,⁹ S. -Y. Fung,⁵ S. Garpman,^{20,*} T. K. Ghosh,⁴⁰
 A. Glenn,³⁶ A. L. Godoi,³³ Y. Goto,³² S. V. Greene,⁴⁰
 M. Grosse Perdekamp,³² S. K. Gupta,² W. Gurny,³
 H. -Å. Gustafsson,²⁰ J. S. Haggerty,³ H. Hamagaki,⁷ A. G. Hansen,¹⁹
 H. Hara,²⁴ E. P. Hartouni,¹⁸ R. Hayano,³⁸ N. Hayashi,³¹ X. He,¹⁰
 T. K. Hemmick,²⁸ J. M. Heuser,²⁸ M. Hibino,⁴¹ J. C. Hill,¹³
 D. S. Ho,⁴³ K. Homma,¹¹ B. Hong,¹⁵ A. Hoover,²⁶ T. Ichihara,^{31,32}
 K. Imai,^{17,31} M. S. Ippolitov,¹⁶ M. Ishihara,^{31,32} B. V. Jacak,^{28,32}
 W. Y. Jang,¹⁵ J. Jia,²⁸ B. M. Johnson,³ S. C. Johnson,^{18,28} K. S. Joo,²³
 S. Kametani,⁴¹ J. H. Kang,⁴³ M. Kann,³⁰ S. S. Kapoor,² S. Kelly,⁸
 B. Khachaturov,⁴² A. Khanzadeev,³⁰ J. Kikuchi,⁴¹ D. J. Kim,⁴³
 H. J. Kim,⁴³ S. Y. Kim,⁴³ Y. G. Kim,⁴³ W. W. Kinnison,¹⁹

E. Kistenev,³ A. Kiyomichi,³⁹ C. Klein-Boesing,²² S. Klinksiek,²⁵
 L. Kochenda,³⁰ V. Kochetkov,¹² D. Koehler,²⁵ T. Kohama,¹¹
 D. Kotchetkov,⁵ A. Kozlov,⁴² P. J. Kroon,³ K. Kurita,^{31,32}
 M. J. Kweon,¹⁵ Y. Kwon,⁴³ G. S. Kyle,²⁶ R. Lacey,²⁷ J. G. Lajoie,¹³
 J. Lauret,²⁷ A. Lebedev,^{13,16} D. M. Lee,¹⁹ M. J. Leitch,¹⁹ X. H. Li,⁵
 Z. Li,^{6,31} D. J. Lim,⁴³ M. X. Liu,¹⁹ X. Liu,⁶ Z. Liu,⁶ C. F. Maguire,⁴⁰
 J. Mahon,³ Y. I. Makdisi,³ V. I. Manko,¹⁶ Y. Mao,^{6,31} S. K. Mark,²¹
 S. Markacs,⁸ G. Martinez,³⁴ M. D. Marx,²⁸ A. Masaïke,¹⁷
 F. Matathias,²⁸ T. Matsumoto,^{7,41} P. L. McGaughey,¹⁹ E. Melnikov,¹²
 M. Merschmeyer,²² F. Messer,²⁸ M. Messer,³ Y. Miake,³⁹
 T. E. Miller,⁴⁰ A. Milov,⁴² S. Mioduszewski,^{3,36} R. E. Mischke,¹⁹
 G. C. Mishra,¹⁰ J. T. Mitchell,³ A. K. Mohanty,² D. P. Morrison,³
 J. M. Moss,¹⁹ F. Mühlbacher,²⁸ M. Muniruzzaman,⁵ J. Murata,³¹
 S. Nagamiya,¹⁴ Y. Nagasaka,²⁴ J. L. Nagle,⁸ Y. Nakada,¹⁷
 B. K. Nandi,⁵ J. Newby,³⁶ L. Nikkinen,²¹ P. Nilsson,²⁰
 S. Nishimura,⁷ A. S. Nyanin,¹⁶ J. Nystrand,²⁰ E. O'Brien,³
 C. A. Ogilvie,¹³ H. Ohnishi,^{3,11} I. D. Ojha,^{4,40} M. Ono,³⁹
 V. Onuchin,¹² A. Oskarsson,²⁰ L. Österman,²⁰ I. Otterlund,²⁰
 K. Oyama,^{7,38} L. Paffrath,^{3,*} A. P. T. Palounek,¹⁹ V. S. Pantuev,²⁸
 V. Papavassiliou,²⁶ S. F. Pate,²⁶ T. Peitzmann,²² A. N. Petridis,¹³
 C. Pinkenburg,^{3,27} R. P. Pisani,³ P. Pitukhin,¹² F. Plasil,²⁹
 M. Pollack,^{28,36} K. Pope,³⁶ M. L. Purschke,³ I. Ravinovich,⁴²
 K. F. Read,^{29,36} K. Reygers,²² V. Riabov,^{30,35} Y. Riabov,³⁰
 M. Rosati,¹³ A. A. Rose,⁴⁰ S. S. Ryu,⁴³ N. Saito,^{31,32} A. Sakaguchi,¹¹
 T. Sakaguchi,^{7,41} H. Sako,³⁹ T. Sakuma,^{31,37} V. Samsonov,³⁰
 T. C. Sangster,¹⁸ R. Santo,²² H. D. Sato,^{17,31} S. Sato,³⁹ S. Sawada,¹⁴
 B. R. Schlei,¹⁹ Y. Schutz,³⁴ V. Semenov,¹² R. Seto,⁵ T. K. Shea,³
 I. Shein,¹² T. -A. Shibata,^{31,37} K. Shigaki,¹⁴ T. Shiina,¹⁹ Y. H. Shin,⁴³
 I. G. Sibiriak,¹⁶ D. Silvermyr,²⁰ K. S. Sim,¹⁵ J. Simon-Gillo,¹⁹
 C. P. Singh,⁴ V. Singh,⁴ M. Sivertz,³ A. Soldatov,¹² R. A. Soltz,¹⁸
 S. Sorensen,^{29,36} P. W. Stankus,²⁹ N. Starinsky,²¹ P. Steinberg,⁸
 E. Stenlund,²⁰ A. Ster,⁴⁴ S. P. Stoll,³ M. Sugioka,^{31,37} T. Sugitate,¹¹
 J. P. Sullivan,¹⁹ Y. Sumi,¹¹ Z. Sun,⁶ M. Suzuki,³⁹ E. M. Takagui,³³
 A. Taketani,³¹ M. Tamai,⁴¹ K. H. Tanaka,¹⁴ Y. Tanaka,²⁴
 E. Taniguchi,^{31,37} M. J. Tannenbaum,³ J. Thomas,²⁸ J. H. Thomas,¹⁸

T. L. Thomas,²⁵ W. Tian,^{6,36} J. Tojo,^{17,31} H. Torii,^{17,31} R. S. Towell,¹⁹
I. Tserruya,⁴² H. Tsuruoka,³⁹ A. A. Tsvetkov,¹⁶ S. K. Tuli,⁴
H. Tydesjö,²⁰ N. Tyurin,¹² T. Ushiroda,²⁴ H. W. van Hecke,¹⁹
C. Velissaris,²⁶ J. Velkovska,²⁸ M. Velkovsky,²⁸ A. A. Vinogradov,¹⁶
M. A. Volkov,¹⁶ A. Vorobyov,³⁰ E. Vznuzdaev,³⁰ H. Wang,⁵
Y. Watanabe,^{31,32} S. N. White,³ C. Witzig,³ F. K. Wohn,¹³
C. L. Woody,³ W. Xie,^{5,42} K. Yagi,³⁹ S. Yokkaichi,³¹ G. R. Young,²⁹
I. E. Yushmanov,¹⁶ W. A. Zajc,⁸ Z. Zhang,²⁸ S. Zhou⁶
(PHENIX Collaboration)

¹*Institute of Physics, Academia Sinica, Taipei 11529, Taiwan*

²*Bhabha Atomic Research Centre, Bombay 400 085, India*

³*Brookhaven National Laboratory, Upton, NY 11973-5000, USA*

⁴*Department of Physics, Banaras Hindu University, Varanasi 221005, India*

⁵*University of California - Riverside, Riverside, CA 92521, USA*

⁶*China Institute of Atomic Energy (CIAE), Beijing, People's Republic of China*

⁷*Center for Nuclear Study, Graduate School of Science, University of Tokyo, 7-3-1 Hongo,
Bunkyo, Tokyo 113-0033, Japan*

⁸*Columbia University, New York, NY 10027 and Nevis Laboratories, Irvington, NY 10533,
USA*

⁹*Florida State University, Tallahassee, FL 32306, USA*

¹⁰*Georgia State University, Atlanta, GA 30303, USA*

¹¹*Hiroshima University, Kagamiyama, Higashi-Hiroshima 739-8526, Japan*

¹²*Institute for High Energy Physics (IHEP), Protvino, Russia*

¹³*Iowa State University, Ames, IA 50011, USA*

¹⁴*KEK, High Energy Accelerator Research Organization, Tsukuba-shi, Ibaraki-ken
305-0801, Japan*

¹⁵*Korea University, Seoul, 136-701, Korea*

¹⁶*Russian Research Center "Kurchatov Institute", Moscow, Russia*

¹⁷*Kyoto University, Kyoto 606, Japan*

¹⁸*Lawrence Livermore National Laboratory, Livermore, CA 94550, USA*

¹⁹*Los Alamos National Laboratory, Los Alamos, NM 87545, USA*

²⁰*Department of Physics, Lund University, Box 118, SE-221 00 Lund, Sweden*

²¹*McGill University, Montreal, Quebec H3A 2T8, Canada*

²²*Institut für Kernphysik, University of Münster, D-48149 Münster, Germany*

²³*Myongji University, Yongin, Kyonggido 449-728, Korea*

²⁴*Nagasaki Institute of Applied Science, Nagasaki-shi, Nagasaki 851-0193, Japan*

²⁵*University of New Mexico, Albuquerque, NM 87131, USA*

²⁶*New Mexico State University, Las Cruces, NM 88003, USA*

²⁷*Chemistry Department, State University of New York - Stony Brook, Stony Brook, NY
11794, USA*

²⁸*Department of Physics and Astronomy, State University of New York - Stony Brook,
Stony Brook, NY 11794, USA*

²⁹*Oak Ridge National Laboratory, Oak Ridge, TN 37831, USA*

- ³⁰*PNPI, Petersburg Nuclear Physics Institute, Gatchina, Russia*
- ³¹*RIKEN (The Institute of Physical and Chemical Research), Wako, Saitama 351-0198, JAPAN*
- ³²*RIKEN BNL Research Center, Brookhaven National Laboratory, Upton, NY 11973-5000, USA*
- ³³*Universidade de São Paulo, Instituto de Física, Caixa Postal 66318, São Paulo CEP05315-970, Brazil*
- ³⁴*SUBATECH (Ecole des Mines de Nantes, IN2P3/CNRS, Universite de Nantes) BP 20722 - 44307, Nantes-cedex 3, France*
- ³⁵*St. Petersburg State Technical University, St. Petersburg, Russia*
- ³⁶*University of Tennessee, Knoxville, TN 37996, USA*
- ³⁷*Department of Physics, Tokyo Institute of Technology, Tokyo, 152-8551, Japan*
- ³⁸*University of Tokyo, Tokyo, Japan*
- ³⁹*Institute of Physics, University of Tsukuba, Tsukuba, Ibaraki 305, Japan*
- ⁴⁰*Vanderbilt University, Nashville, TN 37235, USA*
- ⁴¹*Waseda University, Advanced Research Institute for Science and Engineering, 17 Kikui-cho, Shinjuku-ku, Tokyo 162-0044, Japan*
- ⁴²*Weizmann Institute, Rehovot 76100, Israel*
- ⁴³*Yonsei University, IPAP, Seoul 120-749, Korea*
- ⁴⁴*KFKI Research Institute for Particle and Nuclear Physics (RMKI), Budapest, Hungary[†]*

Abstract

PHENIX has measured the centrality dependence of charged hadron p_T spectra from Au+Au collisions at $\sqrt{s_{NN}} = 130$ GeV. The truncated mean p_T decreases with centrality for $p_T > 2$ GeV/c, indicating an apparent reduction of the contribution from hard scattering to high p_T hadron production. For central collisions the yield at high p_T is shown to be suppressed compared to binary nucleon-nucleon collision scaling of p+p data. This suppression is monotonically increasing with centrality, but most of the change occurs below 30% centrality, i.e. for collisions with less than ~ 140 participating nucleons. The observed p_T and centrality dependence is consistent with the particle production predicted by models including hard scattering and subsequent energy loss of the scattered partons in the dense matter created in the collisions.

1 Introduction

Particle production at large transverse momentum (p_T) provides a new tool to study hot and dense nuclear matter created in high energy nuclear collisions. In nucleon-nucleon collisions, hadrons with $p_T \geq 2$ GeV/c are believed to originate mostly from the jet fragmentation of constituent partons, quarks and gluons, that were scattered with large momentum transfer Q^2 [1]. In nuclear collision these hard scattering processes between constituent partons occur early compared to the lifetime of the strongly interacting matter. Thus the hard scattered partons may traverse the

highest energy density matter produced. Theoretical studies of the propagation of partons in high density matter suggest that they lose a significant fraction of their energy through gluon bremsstrahlung [2] and that the energy lost reflects the density of color charges in the matter through which they pass [3]. The energy loss reduces the momenta of the partons, which results in a corresponding reduction of the momenta of the fragmentation products [4], observable as a reduced yield of high p_T hadrons.

The first measurements of hadron spectra at the Brookhaven National Laboratory Relativistic Heavy Ion Collider (RHIC) facility indicate a suppression of high- p_T hadron production in central Au+Au collisions relative to a binary collision scaling of p+p and $\bar{p} + p$ data [5,6]. No suppression is found for peripheral Au+Au collisions. So far no unique explanation of this apparent absence of the expected jet contribution to the p_T spectrum above 2 GeV/c has been identified.

Models of parton energy loss can reproduce the observed suppression in central Au+Au collisions [7,8,9]. Other final state effects such as re-scattering of hadrons originally produced via the jet fragmentation have been proposed to explain the suppression [10]. It should be noted that models invoking thermal hadron production combined with collective transverse expansion of the reaction volume successfully describe the transverse momentum distributions of identified hadrons up to 3 GeV/c [11,12]. However, the mechanism of equilibration, which requires a reduction of the high p_T particle yield, is not specified in these models.

Alternatively, the initial state may be modified such that the number of hard scatterings is reduced. It is well known that nuclear modifications of the parton distributions exist [13]. These modifications cannot explain the suppression, since in the kinematic range of the measurements anti-shadowing enhances the parton distributions in nuclei [14,15,16]. However, models using a classical QCD picture of a highly relativistic nucleus [17,18] suggest that gluon distributions are saturated for momenta below a scale Q_s and thus reduced compared to expectations based on perturbative QCD [19]. As a consequence, a considerable suppression of hadron production might be expected even well above Q_s [20].

In this letter we present the centrality dependence of the suppression of the high- p_T hadron yield to provide new experimental constraints on theoretical descriptions. These data are complementary to the previous study of the absolute yields [5] and have different systematic errors.

2 Experimental setup and data analysis

The results are obtained from 1.4×10^6 minimum bias Au+Au collisions at $\sqrt{s_{NN}}=130$ GeV recorded by the PHENIX experiment during the Run-1 operation of RHIC

(August - September 2000). Details on the PHENIX detector and its configuration in Run-1 operation can be found in [5,21].

In PHENIX semi-inclusive charged hadron spectra are measured over the range $0.5 < p_T < 5.0$ GeV/c in the east central arm spectrometer using data from a drift chamber (DC) and two segmented cathode pad chambers (PC1 and PC3), located outside of an axial magnetic field at a radial distance of 2.2, 2.5 and 5 m from the beam axis. The detectors cover an azimuthal acceptance of 90° and a pseudo-rapidity range of $|\eta| < 0.35$. In this analysis an additional fiducial cut $|\eta| < 0.18$ is applied to guarantee homogeneous track acceptance for collisions within $|z_{vtx}| < 30$ cm of the nominal interaction point. About $\sim 25\%$ of the azimuthal acceptance is covered by a time-of-flight system which allows proton identification out to 3.5 GeV/c, where the measurement is limited by statistics [22].

A pair of beam-beam counters provides the vertex position along the beam direction (z). Each charged track is reconstructed from the DC measurements of its projection into the bend plane of the magnetic field and two space points provided by PC1 and PC3. The unphysical background, resulting from false associations of drift chamber projections with pad chamber points, is estimated and subtracted by forming artificial events with the locations of pad chamber points inverted around the symmetry axis of the spectrometer. Physical background from decays in flight and photon conversions close to the DC, which only partially traverse the field and thus mimic high momentum tracks, are removed by requiring the track to point back to the event vertex within $|z_{vtx}| < 2.5$ cm. The remaining background level is negligible below 4 GeV/c and less than 40% at 5 GeV/c; this upper estimate is included in the systematic errors.

Corrections of the data are determined by tracing individual particles through a full GEANT simulation, simulating the detector response, then merging this response with that of all particles from a real event and passing the composite event through the PHENIX reconstruction software. The average track reconstruction efficiency in the active detector area is larger than 98% in peripheral collisions and decreases to $68 \pm 6\%$ for central collisions. The corresponding correction is shown on the upper left hand side of Fig. 1. The full correction also depends on p_T . It is plotted for peripheral collision on the upper right hand side of the figure. Between 0.8 and 2.5 GeV/c the correction factor varies slowly with p_T . Its value of ~ 25 corrects for geometrical acceptance ($\Delta\phi = \pi/4$; $\Delta\eta = 0.36$), dead areas of the detectors (45% DC, 5% PC's), and losses due to 2σ track matching cuts. At lower p_T the correction increases reflecting the gradual loss of acceptance. At higher p_T the observed particle yield is artificially increased because of the finite momentum resolution ($\delta p/p \simeq 0.6\% \oplus 3.6\% p$ (GeV/c)) and therefore the correction function decreases. Since this correction depends on the spectral shape of the true p_T distribution it was determined iteratively. At 5 GeV/c the correction is reduced by a factor of ~ 2 . The systematic uncertainties are indicated by the dashed lines; they are also tabulated in Table 1. As shown in the lower part of Fig. 1 correction factorizes into functions of

centrality (i.e. detector occupancy) and p_T within 2% systematic uncertainty in the range from 2 to 5 GeV/c.

Events are selected according to centrality following the procedure described in [5]. Six exclusive centrality bins are established using the energy measured in two zero-degree calorimeters and the number of charged-particles detected in the two beam-beam counters. A Monte-Carlo simulation using measured nucleon density distributions calculated in the Glauber eikonal approximation was used to estimate the average number of binary nucleon-nucleon collisions (N_{coll}) and the corresponding average number of participating nucleons (N_{part}) for each bin. The results are quoted in Table 2.

3 Results

Fig. 2 presents charged hadron p_T spectra for the six centrality bins. For peripheral collisions the spectra are more concave than those for central collisions. This shape difference is seen more clearly by taking the ratio of the spectrum for each centrality bin to the minimum-bias spectrum, as shown on the right hand side of Fig. 2. In these ratios most systematic errors cancel or affect the overall scale only. The ratios for the central bins are almost independent of p_T since central collisions dominate the minimum bias yields. The peripheral bins show a decreasing ratio between 0.5 and 1.5 GeV/c thus in peripheral collisions the yield in this region decreases more rapidly with increasing p_T than in central collisions. For p_T above 1.5 GeV/c this trend is inverted.

Before analyzing the centrality dependence in more detail we demonstrate that the observed suppression of the yield at high p_T does not result from a reduced yield of protons and anti-protons [22]. To evaluate the effect of the (anti-)protons, we plot in the top panel of Fig. 3 the p_T dependence of p/h , the ratio of proton plus anti-proton yields to the total charged hadron yield for minimum bias collisions, which increases steadily. Above 1.5 GeV/c the ratio seem to saturate reaching a value of ~ 0.5 around 3 GeV/c. In the bottom panel of Fig. 3 we show p/h for p_T above 1.8 GeV/c as a function of centrality. Since there is clearly no significant decrease of the p/h ratio with either centrality or p_T , the observed hadron suppression is not due to a larger suppression of the (anti-)proton component than that of the mesons. On the contrary, within the range of the presented measurement the apparent slight increase in p/h with N_{part} could indicate a larger suppression of the meson component relative to all charged hadrons.

To evaluate the change of the hadron spectra more quantitatively we calculate the

truncated average p_T :

$$\langle p_T^{trunc} \rangle \equiv \frac{\int_{p_T^{min}}^{\infty} p_T \cdot dN/dp_T}{\int_{p_T^{min}}^{\infty} dN/dp_T} - p_T^{min} \quad (1)$$

for $p_T^{min} = 0.5$ GeV/c and for $p_T^{min} = 2.0$ GeV/c for each centrality selection ¹. In Fig. 4 $\langle p_T^{trunc} \rangle$ is plotted as a function of N_{part} . The value of $\langle p_T^{trunc} \rangle$ is insensitive to the normalization of the spectra. Systematic uncertainties of $\sim 20(50)$ MeV/c for $p_T^{min} = 0.5(2.0)$ GeV/c result from an 1-2% uncertainty on the momentum scale and the p_T dependent uncertainties on the correction function. Since the centrality and p_T dependence of the correction factorize the error on $\langle p_T^{trunc} \rangle$ is independent of centrality to better than 2 MeV/c.

The $\langle p_T^{trunc} \rangle$ for $p_T^{min} = 0.5$ GeV/c increases with N_{part} similar to the average p_T of identified charged hadrons [22]. For higher $p_T^{min} = 2.0$ GeV/c the $\langle p_T^{trunc} \rangle$ drops by ~ 60 MeV/c with N_{part} , distinctly different from the expected increased role of hard particle production in the more central collisions. Absent any collective effects, the hard scattering contribution should increase relative to soft production by the factor N_{coll}/N_{part} which grows from 1.5 to ~ 6 from peripheral to central collisions. Since the relative contribution of the hard component to the spectrum increases with p_T , this should lead to a rise of $\langle p_T^{trunc} \rangle$ for sufficiently large p_T^{min} . The drop of $\langle p_T \rangle$ therefore indicates the suppression of the high p_T relative to the low p_T hadron yield independent of systematic errors associated with the absolute normalization of the spectra or any nucleon-nucleon reference distribution.

Changes of the hadron spectra at high p_T are often presented in terms of the nuclear modification factor R_{AA} . This measure relies on the absolute normalization and a reference and therefore has intrinsically larger systematic uncertainties, but it allows to quantify the suppression. We have calculated R_{AA} for each centrality bin as:

$$R_{AA}(p_T, \eta) = \left(\frac{1}{N_{evt}} \frac{d^2 N^{A+A}}{dp_T d\eta} \right) / \left(\frac{\langle N_{coll} \rangle}{\sigma_{inel}^{N+N}} \frac{d^2 \sigma^{N+N}}{dp_T d\eta} \right) \quad (2)$$

For the N+N charged hadron cross section we use a power-law parameterization $1/\pi d^2\sigma/dp_T^2 = A/(1 + p_T/p_0)^n$, with $A = 330$ mb/(GeV/c)², $p_0 = 1.72$ GeV/c, and $n = 12.4$. The parameters were obtained by interpolating p+p and \bar{p} +p data to $\sqrt{s} = 130$ GeV as described in [5]. In Fig. 5 the $R_{AA}(p_T)$ values for all centrality bins excluding the most peripheral one are compared to the central (0-5%) bin. The systematic uncertainties in the normalization of the data, in N_{coll} , and in the N+N

¹ The value of $\langle p_T^{trunc} \rangle$ is closely related to the local inverse slope which is slightly smaller. The conversion to local slope depends on the spectral shape and also on p_T^{min} . For an exponential spectrum with an inverse slope of 350 MeV/c the conversion is approximately $-80(-60)$ MeV/c for $p_T^{min} = 0.5(2.0)$ GeV/c.

reference (20%) result in overall systematic errors of about 41%, 34%, 31%, 31% and 30% for centrality bins 2-6, respectively. The errors are quoted for the range from 1 to 3.5 GeV/c; they increase somewhat towards higher p_T . Comparing R_{AA} for a given centrality bin to the most central bin, the systematic errors reduce to $\sim 6\%$ for bin 5 (5-15%) and nearly 27% for bin 2(60-80%). They are dominated the uncertainty in N_{coll} listed in Table 2.

For the 60-80% centrality bin, R_{AA} increases with p_T and reaches unity at high p_T . In comparison to the 60-80% bin, the R_{AA} values for the most central bin remain significantly below unity at a value of 0.55 for $p_T > 2$ GeV/c. At high p_T approximately constant R_{AA} values are detected in all centrality bins. The high p_T values decrease monotonically with centrality, clearly indicating that the magnitude of the suppression of high p_T hadrons increases with centrality. This is shown clearly in the upper part of Fig. 6, which presents R_{AA} obtained for the three p_T bins 1.6 to 2.6 GeV/c, 2.6 to 3.6 GeV/c, and above 3.6 GeV/c as a function of centrality. For central collisions we observe a suppression of about a factor of 2 ± 0.6 compared to binary collision scaling. Relative to peripheral collisions the suppression factor in central collisions increases with p_T from 1.25 ± 0.2 to 1.5 ± 0.2 to 1.8 ± 0.3 for the three p_T bins, respectively.

We note that for peripheral collisions the data do not indicate a significant increase of R_{AA} above unity, unlike data at lower energies [23]. However, such an increase, attributed to initial state scattering, the Cronin effect [24], may well be consistent with the peripheral data due to the large systematic uncertainty of the R_{AA} scale. While the relative difference between the peripheral and central spectra increases with p_T , the roughly constant nuclear modification factor at large p_T suggests an approximately p_T independent suppression of hard scattering contributions over the range $2 < p_T < 4.5$ GeV/c.

The physics that controls the production of high- p_T particles or the suppression of the hard scattering yields in the measured p_T range may not depend directly on N_{coll} . Thus, we have calculated a different ratio, R_{AA}^{part} , defined similarly to R_{AA} but with N_{coll} replaced by the number of participant pairs, $N_{part}/2$. If particle production increases proportional to the number of participants, $R_{AA}^{part} = 1$.

The obtained R_{AA}^{part} values are shown in Fig. 6 (bottom) for the three p_T bins used above. The values of R_{AA}^{part} are larger than R_{AA} by a factor equal to $2N_{coll}/N_{part}$ the average number of nucleon-nucleon collisions suffered by each participant. For all p_T bins the yield per participant is consistent with unity for peripheral collisions as expected since peripheral collisions should closely resemble N+N collisions. For central collisions R_{AA}^{part} increases to approximately three. Most of this change occurs in the range of N_{part} from 40 to 140. For larger N_{part} the yield in the highest p_T bin is approximately constant while in both lower p_T bins it increases by 20 to 30%.

4 Concluding discussion

In this paper we have presented the centrality dependence of charged hadron p_T spectra focusing on the behavior of the spectra at high p_T . A striking change of the spectral shape is observed when comparing spectra from different centrality selections. For peripheral collisions the spectrum exhibits a pronounced concave shape which is modified towards a more exponential spectrum as the centrality increases. The observed lack of variation with centrality in the proton to charged ratio at large transverse momenta indicates that the modification is not due to a change in the relative yields of protons.

We observe a decrease of $\langle p_T^{trunc} \rangle$ for $p_T > 2$ GeV/c with increasing centrality, which is distinctly different from the increase of $\langle p_T \rangle$ and demonstrates the suppression of the high p_T hadron yield independent of systematic errors associated with the absolute normalization of the spectra. The data are not consistent with binary collision scaling of hard scattering processes, which would result in an increase of $\langle p_T^{trunc} \rangle$. If the p_T spectra above 2 GeV/c are strongly affected by collective motion of matter before freeze-out, we would also expect an increase $\langle p_T^{trunc} \rangle$ since the corresponding flow velocities should increase in more central collisions [25]. Similarly, if gluon saturation is important for particle production in the p_T range above 2 GeV/c, $\langle p_T^{trunc} \rangle$ should increase with increasing N_{part} due to the predicted logarithmic increase of Q_s [26]. In contrast, the data are consistent with models assuming energy loss of hard scattered partons, which results in an increasing reduction of the hard scattering contribution to the hadron spectrum with increasing centrality of the collisions [7,8,9]. It remains to be seen whether this explanation is unique.

Comparing the measured differential yields in five centrality bins to an N_{coll} scaling of the N+N reference yields we see a suppression of the yields in central collisions at high p_T , consistent with the results in [5,6]. In the 0-30% centrality range (bins 1-3) the suppression is approximately independent of p_T for $2 < p_T < 5$ GeV/c at a value of $R_{AA} \sim 0.6$ and simultaneously nearly independent within 20% of centrality. The suppression sets in gradually with the largest change occurring over the 30-60% centrality range. This centrality bin covers a broad range of collision geometries. Whether the change is continuous or exhibits a threshold behavior, as predicted in [27], cannot be judged from the present data. The observed suppression is consistent with parton energy loss scenarios. In these models, the value of R_{AA} and its p_T dependence are very sensitive to the actual energy loss prescription. Due to the large systematic errors on the R_{AA} scale, the contribution from the protons and the limited p_T reach of the data presented here, we can not distinguish between the different energy loss prescriptions on the basis of R_{AA} .

In summary, a detailed analysis of the centrality dependence of charged particle data from Au-Au collisions at $\sqrt{s_{NN}} = 130$ GeV measured by PHENIX reveals

interesting features of the observed high p_T hadron suppression. The decrease of the average p_T with increasing centrality seems to favor models of particle production that consider energy loss effects, rather than saturation- or hydrodynamics-based approaches for this p_T range. The suppression sets in gradually with the largest changes occurring for peripheral collisions with less than about 140 participating nucleons. From there on it does not change substantially towards more central collisions.

Acknowledgements

We thank the staff of the Collider-Accelerator and Physics Departments at BNL for their vital contributions. We acknowledge support from the Department of Energy and NSF (U.S.A.), MEXT and JSPS (Japan), RAS, RMAE, and RMS (Russia), BMBF, DAAD, and AvH (Germany), VR and KAW (Sweden), MIST and NSERC (Canada), CNPq and FAPESP (Brazil), IN2P3/CNRS (France), DAE and DST (India), KRF and CHEP (Korea), the U.S. CRDF for the FSU, and the US-Israel BSF.

Note Added in Proof

After submission of our manuscript, data from Au-Au collisions at $\sqrt{s_{NN}} = 200$ GeV were presented by the PHOBOS collaboration[28,29], with an emphasis on the lack of variation in the scaled yields with N_{part} for $N_{part} > 65$. Keeping in mind that results from different energies are not directly comparable, we note that the broader range in N_{part} presented here shows that this effect does not apply over the entire range of centralities, and that when normalized with the appropriate p-p yields, is simply an aspect of the smooth variation of R_{AA}^{part} visible in Fig. 6.

References

[*] Deceased

[†] Not a participating Institution.

- [1] H.Jöstlein et al., Phys. Rev. **D20** (1979) 53.
- [2] M. Gyulassy and M. Plümer, Phys. Lett. **B243** (1990) 432; X.N. Wang and M. Gyulassy, Phys. Rev. Lett. **68** (1992) 1480.
- [3] X.N. Wang, M. Gyulassy and M. Plümer, Phys. Rev. **D51** (1995) 3436; R. Baier et al., Phys. Lett. **B345** (1995) 277; R. Baier, D. Schiff and B.G. Zakharov, Ann. Rev. Nucl. Part. Sci. **50** (2000) 37-69.
- [4] M. Gyulassy and X.N. Wang, Nucl. Phys. **B420** (1994) 583; X.N. Wang, Phys. Rev. **C58** (1998) 2321.

- [5] PHENIX Collaboration: K. Adcox et al., Phys. Rev. Lett. 88 (2002) 22301.
- [6] STAR Collaboration: C. Adler et al., Phys. Rev. Lett. 89 (2002) 202301.
- [7] X.N. Wang Phys. Rev. C61 (2000) 64910.
- [8] M. Gyulassy, P. Levai and I. Vitev, Phys. Rev. Lett. 85 (2000) 5535.
- [9] P. Levai et al., Nucl. Phys. A698 (2002) 631.
- [10] K. Gallmeister, C. Greiner, and Z. Xu, nucl-th/0202051.
- [11] P. Kolb et al., Nucl. Phys. A696 (2001) 197.
- [12] D. Teaney, J. Lauret and E.V. Shuryak, nucl-th/0110037.
- [13] J.J. Aubert et al., Phys. Lett. B123, (1983) 275.
- [14] L.V. Gribov, E.M. Levin and M.G. Ryskin, Phys. Repts. 100 (1983) .
- [15] Z. Huang, H. J. Lu and I. Sarcevic, Nucl. Phys. A637 (1998) 79.
- [16] K.J. Eskola, V.J. Kolhinen and C.A. Salgado, Eur.Phys.J. C9 (1999) 61.
- [17] L. D. McLerran and R. Venugopalan, Phys. Rev. D49 (1994) 2233.
- [18] A. Kovner, L. D. McLerran and H. Weigert, Phys. Rev. D52 (1995) 6231.
- [19] A. Krasnitz, Y. Nara and R. Venugopalan, Phys. Rev. Lett. 87 (2001) 192302.
- [20] D. Kharzeev, E. Levin and L. D. McLerran, hep-ph/0210332.
- [21] PHENIX Collaboration: K. Adcox et al., Phys. Rev. Lett. 86 (2001) 3500 and Phys. Rev. Lett. 87 (2001) 052301.
- [22] PHENIX Collaboration: K. Adcox et al., Phys. Rev. Lett. 88 (2002) 242301.
- [23] E. Wang and X. N. Wang, nucl-th/0104031 and references therein.
- [24] D. Antreasyan *et al.*, Phys. Rev. D19 (1979) 764.
- [25] E. Shuryak private communication.
- [26] D. Kharzeev and E. Levin, nucl-th/0108006, J. Schaffner-Bielich et al., nucl-th/0108048.
- [27] X.N. Wang, Phys. Rev. C63 (2001) 54902.
- [28] PHOBOS Collaboration: C. Roland et al., arXiv:hep-ex/0212006.
- [29] PHOBOS Collaboration: B. B. Back et al., arXiv:nucl-ex/0302015, submitted to Phys. Lett. B.

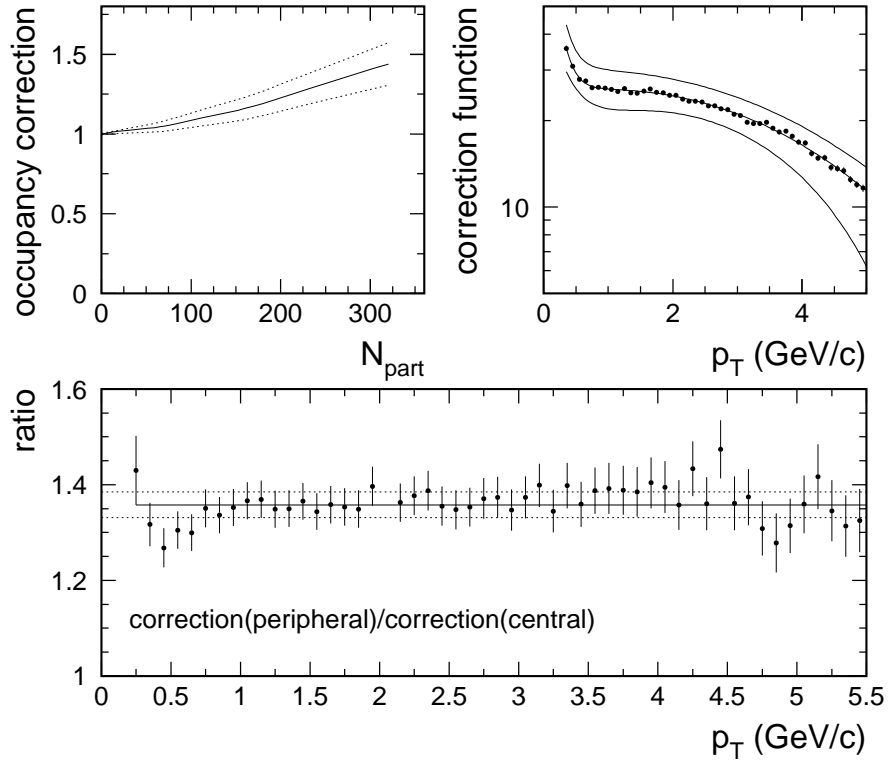


Fig. 1. Functions used to correct the charged particle p_T spectra. Upper left panel shows the centrality dependent correction $c(N_{part})$ and the right panel shows the p_T dependent correction $c(p_T)$. The systematic uncertainties are indicated by the dashed lines. The two corrections factorize, so that for any centrality the full correction function is given by $c(p_T) \times c(N_{part})$. The accuracy of this factorization is demonstrated in the lower panel. The ratio of the full correction for central collisions (top 5%) to the correction for single particle events varies by less than 2% above 1 GeV/c.

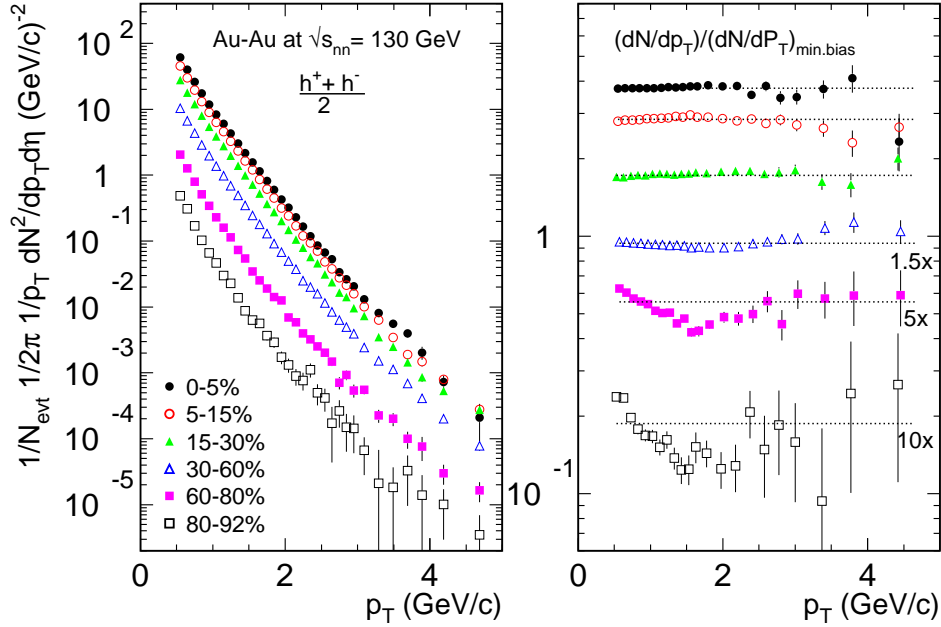


Fig. 2. The left panel shows p_T spectra of charged hadrons from six Au+Au centrality selections. Error bars indicate statistical errors only. The p_T dependent systematic errors are independent of centrality and not shown, they are given in Table 1. The centrality dependent errors are less than 10% and small compared to the symbol size. The right panel shows the ratio of each of the centrality selected p_T spectra to the minimum bias spectrum. Ratios for peripheral selections are scaled for clarity. Dotted lines indicate the average ratios for each centrality selection.

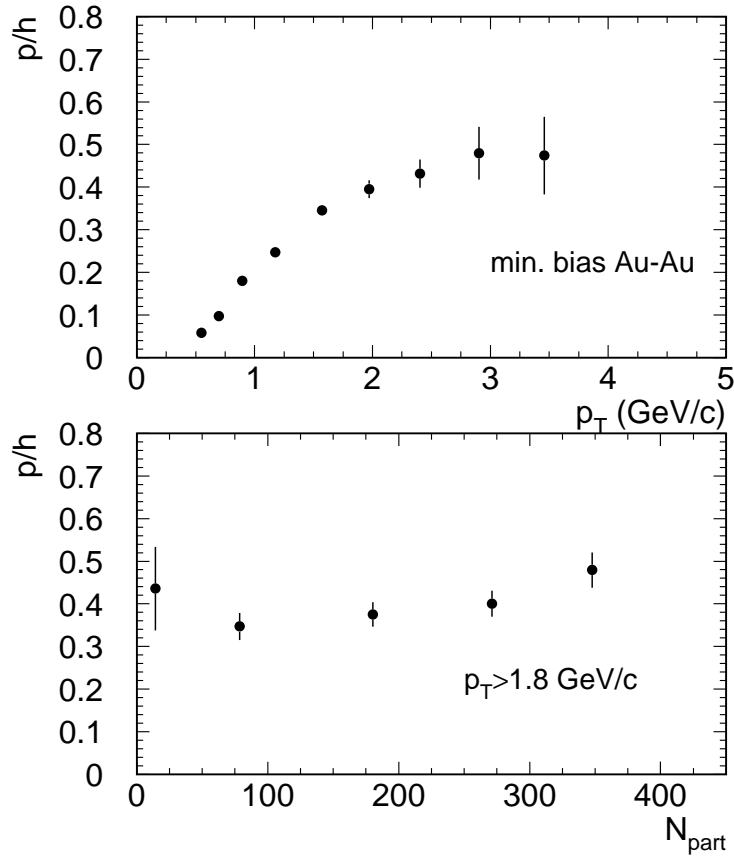


Fig. 3. The ratio p/h represents the proton plus anti-proton yield relative to the total charged hadron multiplicity. The top panel shows the p_T dependence of p/h for minimum bias events. In the bottom panel we show the centrality dependence of p/h for $p_T > 1.8$ GeV/c. Only statistical errors are shown.

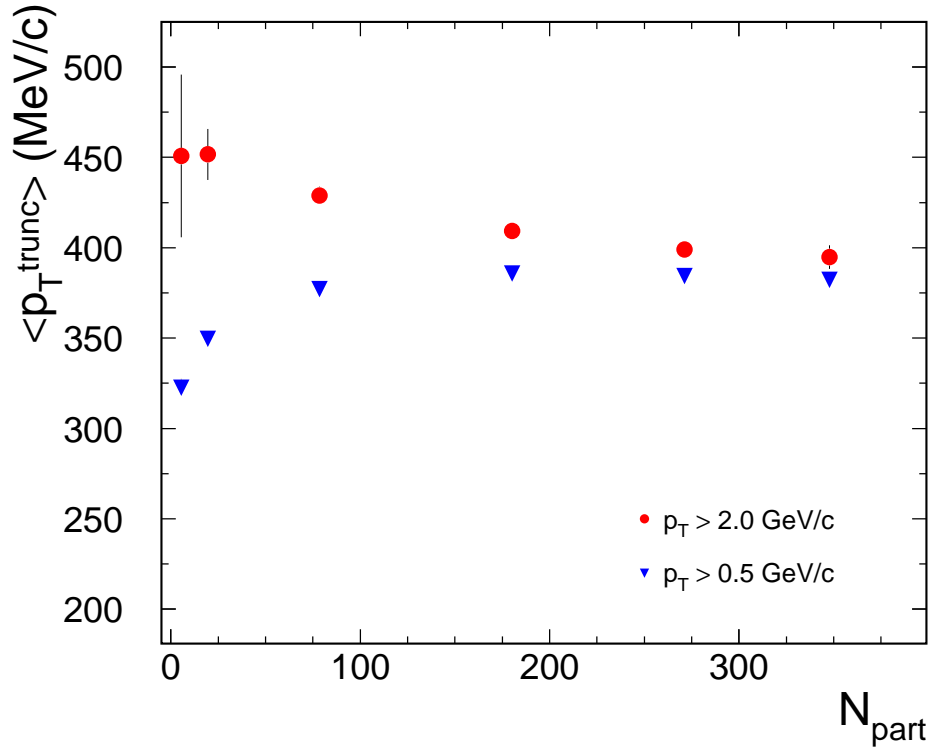


Fig. 4. Centrality dependence of $\langle p_T^{trunc} \rangle$, the average p_T of charged particles with p_T above a threshold p_T^{min} minus the threshold p_T^{min} . Shown are values for two p_T^{min} cuts, one at $p_T > 0.5$ GeV/c representing all data presented in Fig. 2 and the other one at $p_T > 2$ GeV/c. Only statistical errors are shown; see the text following Eq. 1 for a discussion of the systematic errors.

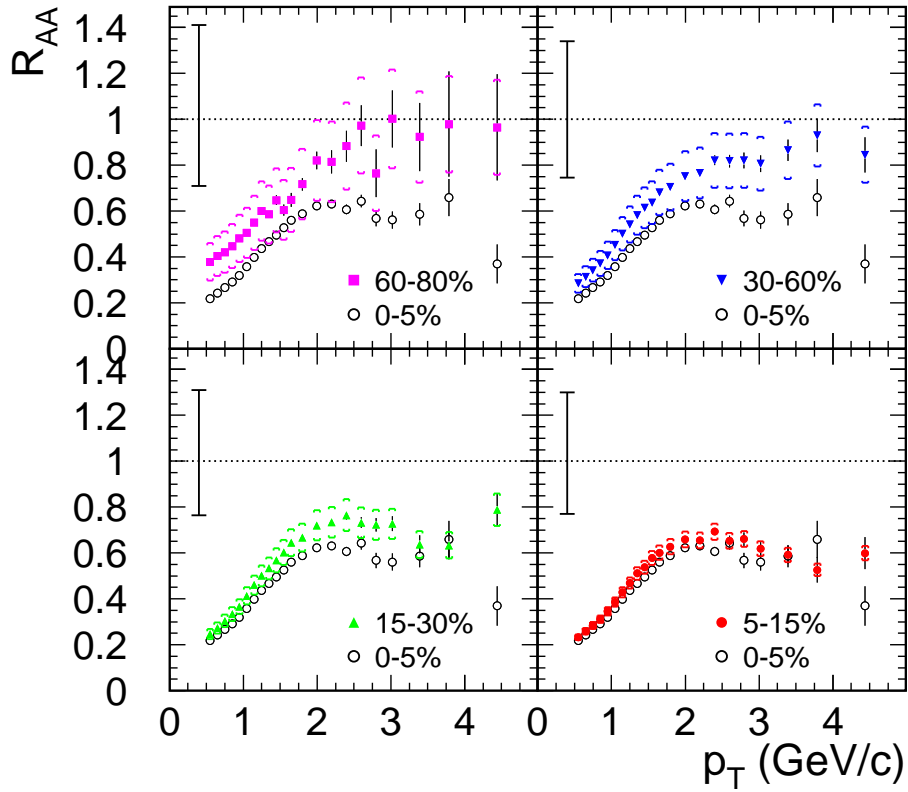


Fig. 5. Nuclear modification factor (R_{AA}) for the 60-80%, 30-60%, 15-30%, and 5-15% centrality selections compared to the one for the most central sample (0-5%). Due to insufficient statistics R_{AA} is not shown for the 80-92% sample. The solid error bars on each data point are statistical. The systematic error between the more peripheral and the central sample are given as brackets for the more peripheral data points. The error bar on the left hand side of each panel indicates the overall systematic error on the R_{AA} scale.

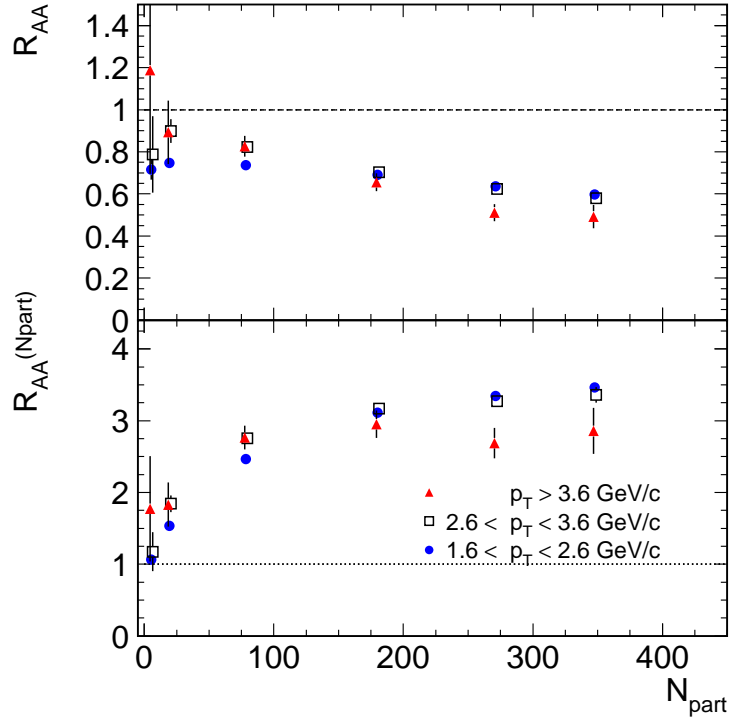


Fig. 6. The top panel gives the nuclear modification factor R_{AA} for three exclusive p_T regions as a function of the centrality of the collision. The lower panel shows essentially the same quantity but normalized to the number of participant pairs rather than to the number of binary collisions. The dotted line indicates the expectation for scaling with the number of binary collisions (top) or with the number of participants (bottom). Only statistical errors are shown. The systematic error on the scale and the centrality dependence are identical to the errors shown in Fig. 5. These errors are correlated, i.e. take their maximum or minimum value simultaneously for all centrality and p_T selections. In addition, there are also p_T dependent systematic errors, which are given in Table 1. The systematic errors do not alter the trends in the data.

p_T (GeV/c)	δ_{track} (%)	δ_{decay} (%)	δ_{reso} (%)	δ_{bgr} (%)	total
1	± 13.5	+ 10	± 0	0	-13.5 +16.4
2	± 13.5	+ 5	± 1	0	-13.7 +14.4
3	± 13.5	+ 2.5	± 4	-1.6	-14.2 +14.2
4	± 13.5	+ 1.25	± 9	-11.5	-20 +16
5	± 13.5	+ 0.6	± 15	-40	-45 +20

Table 1

Upper bounds of the systematic error on the p_T dependent single particle correction function. Here δ_{track} includes the uncertainties of the acceptance, dead areas, track matching cuts and the track reconstruction efficiency. The δ_{decay} term accounts for the uncertainty of the decay correction. The effect of the momentum resolution contributes with δ_{reso} to the systematic error. Uncertainties due to potentially unsubtracted background are quantified by δ_{bgr} . The total systematic error given in the last column is calculated as quadrature sum of the individual contributions. It is calculated separately for positive and negative errors.

bin	relative fraction	N_{part}	N_{coll}	$N_{coll}^{central}/N_{coll}$	$2N_{coll}/N_{part}$
1	80-92%	5.5 ± 2.6	4.1 ± 1.7	246 ± 98	1.5 ± 0.5
2	60-80%	19.5 ± 3.5	20 ± 6	50.4 ± 13	2.1 ± 0.5
3	30-60%	79 ± 4.6	131 ± 23	7.68 ± 1.1	3.4 ± 0.6
4	15-30%	180 ± 6.6	406 ± 46	2.49 ± 0.13	4.5 ± 0.5
5	5-15%	271 ± 9	712 ± 72	1.41 ± 0.03	5.2 ± 0.6
6	0-5%	348 ± 10	1009 ± 101	1	5.8 ± 0.6

Table 2

Number of participants and binary collisions and their systematic errors for the individual centrality selections used in this analysis. Also given is the ratio of the number of binary collisions for the most central sample relative to the one for each sample. The last column quantifies the ratio of binary collisions to participant pairs.